Available online at www.sciencedirect.com
ScienceDirect
Journal of Solid State Chemistry 180 (2007) 3093–3100
JOURNAL OF SOLID STATE CHEMISTRY
www.elsevier.com/locate/jssc

Microstructure and electrical transport in nano-grain sized $Ce_{0.9}Gd_{0.1}O_{2-\delta}$ ceramics

Enrique Ruiz-Trejo[a,*], Jaime Santoyo-Salazar[a], Ruben Vilchis-Morales[a], Adriana Benítez-Rico[a], Francisco Gómez-García[a], Carlos Flores-Morales[b], José Chávez-Carvayar[b], Gustavo Tavizón[a]

[a]*Departamento de Física y Química Teórica, Facultad de Química, Universidad Nacional Autónoma de México, México, D.F., 04510, México*
[b]*Instituto de Investigaciones en Materiales, Universidad Nacional Autónoma de México, México, D.F., 04510, México*

Received 30 May 2007; received in revised form 21 August 2007; accepted 22 August 2007
Available online 14 September 2007

Abstract

An enhancement of the electrical conductivity has been found in nano-grain sized $Ce_{0.9}Gd_{0.1}O_{2-\delta}$ ceramics when measured in N_2 ($p_{O_2} = 3.5 \times 10^{-6}$ atm) in comparison with the most commonly accepted values of bulk ionic conductivity. We first present the synthesis and characterisation of the nanoparticles later used for the preparation of dense nanoceramics of Gd-doped CeO_2. The nanoparticles were characterised by X-ray diffraction (XRD), atomic force microscopy (AFM) and transmission electron microscopy (TEM). The good sintering properties of these nanopowders allowed us to obtain very dense ceramics (>90% theoretical density) while keeping the grain size close to 100 nm. The microstructure of these nanoceramics was analysed by AFM and scanning electron microscopy (SEM) while the electrical characterisation was performed by the 4-point dc technique between 500 and 950 °C in air or N_2 and ac impedance between 150 and 400 °C in air and or argon. We briefly discuss the possibilities of electron vs. oxygen ion conduction and grain boundary vs. bulk conductivity. The features exhibited by these ceramics represent an increased potential to process solid electroceramics materials with specific levels of electronic and/or ionic conductivities for a variety of electrochemical devices.

Keywords: Gd-doped Ceria; Nanoparticles; Combustion synthesis; Nanoceramics; Conductivity

1. Introduction

Pure ceria and ceria-based materials present an interesting range of electric transport properties. It has been known for many years that high purity ceria is an n-type semiconductor [1] and that this has a polaronic nature in very reducing conditions and at high temperatures after the loss of oxygen [2]. The doping of cerium oxide in the series $Ce_{1-x}Ln_xO_{2-x/2}$ (Ln = lanthanides^{3+} or Y^{3+}, $x = 0.1, 0.2, 0.3$) produces its characteristic high oxygen-ion mobility [3]. However, this series can also exhibit electronic or mixed ionic-electronic conduction in reducing atmospheres [4–6]. Electronic conduction can also appear when the grain size of non-doped ceria is below 100 nm [7–10]. Nevertheless, the electronic and ionic conductivity in nanograin-sized heavily doped ceria is not yet thoroughly studied and here lies the possibility of more applications in electrochemical devices.

Cerium oxide has a fluorite structure that is generally regarded as quite tolerant to the introduction of aliovalent dopants. The appropriate doping of the cerium oxide lattice with gadolinium oxide as a dopant can be written, in the Kröger-Vink [11] notation, as

$$Gd_2O_3 + 2Ce_{Ce}^{x} + O_O^{x} \rightarrow 2Gd'_{Ce} + V_O^{\bullet\bullet} + 2CeO_2. \quad (1)$$

These oxygen vacancies promote the oxygen-ion migration that is characteristic of doped ceria. It is also known that a high concentration of oxygen vacancies eventually decreases the conductivity, and increases the activation energy [12].

The reduction of the cerium oxide takes place at low partial pressures of oxygen. Thus, the loss of oxygen in the

*Corresponding author. Fax: +52 55 56 22 35 21.
E-mail address: enrique.ruiz_trejo@servidor.unam.mx (E. Ruiz-Trejo).

0022-4596/$ - see front matter © 2007 Elsevier Inc. All rights reserved.
doi:10.1016/j.jssc.2007.08.030

lattice can be written as

$$O_O^x \rightleftarrows V_O^{\bullet\bullet} + 2e' + 1/2O_{2(g)}. \quad (2)$$

The excess electrons are usually associated with Ce^{3+} cations. Electron migration takes place when electrons hop from Ce^{3+} to Ce^{4+} atoms in the crystal lattice, a mechanism known as polaron transport. In this context, the dopant cation does not participate actively in this type of transport.

It is the ability of Ln^{3+}-doped CeO_2 to have largely ionic conduction under certain conditions that makes this series of compounds serious candidates for a variety of high temperature electrochemical devices such as electrically driven oxygen separation membranes [13], solid oxide electrolysis cells (SOEC) [14] and solid oxide fuel cells (SOFC) [15]. It is, on the other hand, the ability to have mixed ionic-electronic conduction under other conditions what opens the possibility of using it as a pressure-driven oxygen separation membrane [16,17] or as an anode for a SOFC [18].

The electrical properties of heavily doped ceria with nano-sized grains are currently under investigation in different laboratories around the world. For example, it has been anticipated that at 500 °C the boundary between ionic and electronic regime will be observed at a grain size of 20 nm [19]. There are recent claims that the ionic conductivity of $Ce_{0.8}Ln_{0.2}O_{2-\delta}$ (Ln = Sm, Y) increases with decreasing grain size at temperatures below 200°C [20,21]. A clear dependence of dc conductivity with grain size for Y-doped CeO_2 has also been reported [22] while we have observed an enhancement in conductivity for Y-doped CeO_2 [23] in relatively mild reducing conditions of nitrogen gas. There are also indications that a decreasing grain size induces an increasing electronic conductivity [24].

The preparation of dense membranes is a key point for some technological application of Ln^{3+}-doped ceria. A membrane with a low porosity is needed to be used as an electrolyte in SOFC and separation membranes. For a long time, the standard procedure to prepare dense samples of doped ceria involved high temperature (>1500 °C) annealing [25]; this introduces problems associated with the processing of a final device such as unwanted cation diffusion between different components, expensive high temperature treatments and evaporation of materials. However, the situation has changed over the years, and recent reports indicate that high density specimens can be prepared at lower temperatures <1300 °C [26,27] when starting from nanopowders; furthermore, the low temperature treatments keep the grains small providing, therefore, a tool for the tailoring of material properties. In this work we have used the combustion synthesis method to obtain dense materials with small grain size.

In this article, we explore the microstructure and electrical conductivity of nanoceramics of gadolinium-doped cerium oxide to investigate their potential as materials for electrochemical devices. First we concentrate on the synthesis and characterisation of the nanoparticles and then on the preparation and electrical properties of a dense sample with nano-sized grains. We hypothesise that the conductivity can be modified by controlling the grain size and, in this way we should be able to design in the near future a material with specific electronic and/or ionic conductivity.

2. Experimental

2.1. Synthesis of nanoparticles

Nanoparticles of $Ce_{0.9}Gd_{0.1}O_{2-\delta}$ were prepared by combustion synthesis [26] starting from the appropriate stoichiometric mixture of $Ce(NO_3)_3 \cdot 6H_2O$ (Aldrich, 99.9%) and $Gd(NO_3)_3 \cdot 6H_2O$ (Aldrich, 99.9%) as the oxidising compounds and glycine (Aldrich, >99%) as the reducing agent. The exact cation content in each nitrate was checked by weighing the nitrate, decomposing it in an oven and weighing the remaining oxide. A ratio of 0.56 glycine/nitrates was used in order to obtain the optimum reaction conditions [26]. A humid paste was formed after mixing the compounds in an agate mortar in air. The excess water was eliminated on a hot plate just below 100 °C and then the temperature was increased until spontaneous combustion took place. For safety, only approximately 5 g of material were prepared per batch. The collected powder was crumbled easily with the mortar and heated in an alumina crucible at 550 °C for 1 h to eliminate organic residues.

2.2. Preparation of nanoceramics

We prepared pellets of 1 mm height and 13 mm diameter by pressing the nanopowders uniaxially (268 MPa) in a steel die. We performed then a variety of tests in order to find the optimal condition for sintering. These specimens were heated with different ramps and at different temperatures (1000–1350 °C) and times (5 min up to 4 h) in air ($p_{O_2} = 0.16$ atm in Mexico City).

2.3. Microstructure

The powder topology was analysed by atomic force microscopy (AFM) (JEOL JSPM-4210 Scanning Probe Microscope) in Tapping™ mode with Ultrasharp tips (CSC 21/25–NSC 15/25 Ultra–Sharp silicon cantilevers) under normal pressure conditions. The powder morphology was studied by transmission electron microscopy (TEM) (JEOL JEM 1200EX). Interplanar distances d were obtained using $dR = \lambda L$ by where R is the radius of the circle of the diffraction pattern, L the constant of the camera (100 cm) and λ is the wavelength (0.0034 Å–120 V).

An X-ray diffraction (XRD) (Siemens D5000, Cu$K\alpha$ radiation) study was performed to check the phase purity of the nanopowders. Scherrer's formula was used to determine the particle size using NaCl as a standard to determine the instrumental broadening [28]. We followed

the growth of the particles by XRD *ex-situ* after annealing the nanopowders for 3 h at different temperatures.

We analysed the microstructure of the nanoceramics by scanning electron microscopy (SEM) (JEOL Leica-Cambridge, Stereoscan 440) and AFM while the phase purity in the pellets was checked by XRD. The densities of the nanoceramics were determined by the Archimedes' method using de-ionised water as the immersion fluid.

2.4. Electrical conductivity

Four-point dc conductivity (Lakeshore 120 Current Source, Agilent 34401A Multimeter) was used to obtain the total conductivity of these materials. We cut out small bars from the pellets to be used for the dc measurements. Four Pt wires (0.25 mm diameter) and Pt paint were used (Tanaka Kikinzoku Kogyo KK TR-7905) as the electrodes after annealing at 700 °C for 3 h. We used two different gas atmospheres: nitrogen ($p_{O_2} = 3.5 \times 10^{-6}$ atm) and air ($p_{O_2} = 0.16$ atm) for the measurements. The oxygen content in N_2 was given by the manufacturer. The partial pressures of oxygen already take into account the average atmospheric pressure in Mexico City. The N_2 was humidified ($p_{H_2O} = 0.011$ atm) to improve the reaction of oxygen incorporation/evolution at the electrodes [29]. We applied a current and measured the voltage as a function of time until a stable value was obtained (ca. 5 min). We then changed the current and repeated the procedure to ensure that the behaviour was ohmic at each temperature. From a plot of V vs. I we estimated the resistance from the slope of the line obtained. All the voltages measured were always below 1 V. The lowest temperature used in this measurement was 750 °C as no stable measurement was attained below this value in a nitrogen atmosphere. The highest limit was arbitrarily set to 950 °C in order to avoid excessive coarsening of the materials.

We used a simple ac measurement (HP4192A Impedance Analyser) in the frequency range 5–13 MHz to investigate the electrical properties in the lower temperature regime (150–300 °C) in air and argon (5×10^{-6} atm). The semicircles obtained were fitted using a non-linear square fitting to a simple RC or RC–RC circuit [30] to estimate the virtual intercept with the real axis. We used the total conductivity as obtained from the impedance measurements to compare with the high temperature 4-point dc conductivity data.

4. Results

4.1. Nanoparticles

The vigorous combustion yields nanoparticles of relative good homogeneity. The diffraction peaks led to the identification of a pure phase $Ce_{0.9}Gd_{0.1}O_{2-\delta}$ with fluorite structure and to the recognition that the Gd was readily incorporated into the lattice with no other secondary phase visible see Fig. 1. The wide base of peaks is characteristic of

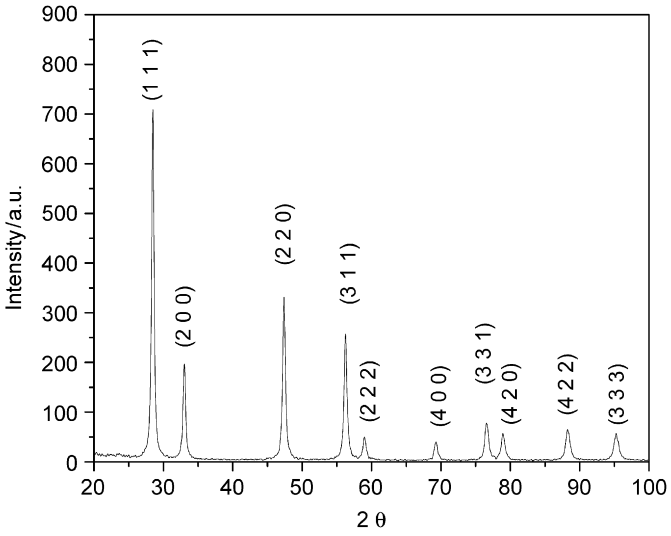

Fig. 1. A diffraction pattern of $Ce_{0.9}Gd_{0.1}O_{2-d}$ showing a perfect fluorite structure.

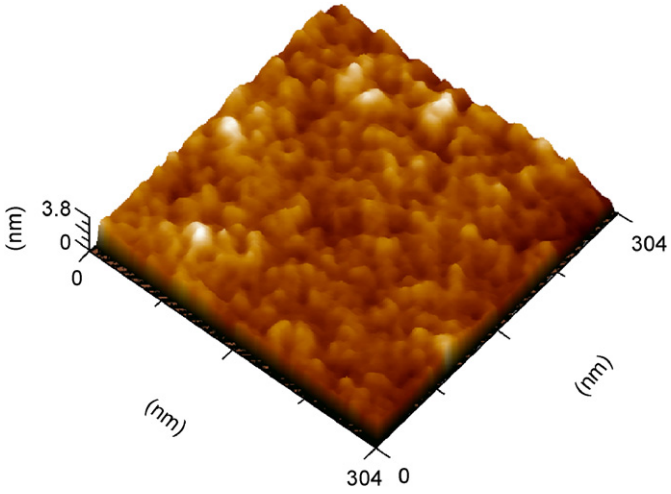

Fig. 2. 3D topological image of $Ce_{0.9}Gd_{0.1}O_{2-d}$.

the small size particles. We estimated a particle size average of 19 nm.

Fig. 2 presents an AFM image of the nanoparticles. The topography observed in Fig. 2 shows a relative homogeneous particle size distribution in a scanned area of 304×304 nm. The image indicates a planar roughness of approximately 3.5 nm and close contact between the nanoparticles. A rough estimation of the particle size in a scanned area of 200×200 nm yields an average of 21 nm.

Fig. 3 shows a TEM micrograph of a batch of $Ce_{0.9}Gd_{0.1}O_{2-\delta}$ particles taken at 300KX. The average particle size is of the order of 20 nm. A detailed zoom was done in order to resolve some rows of atoms inside a nanoparticle. This image gives a better idea of the shape and size of the individual particles, and shows a more polyhedric nature as opposed to the round particles of the Y-doped CeO_2 [23].

Fig. 4 shows an electron diffraction pattern of the $Ce_{0.9}Gd_{0.1}O_{2-\delta}$ nanoparticles in a selected area. The

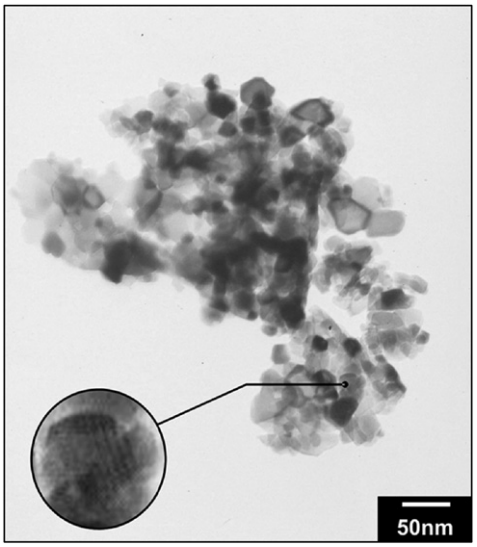

Fig. 3. $Ce_{0.9}Gd_{0.1}O_{2-d}$ nanoparticles observed by TEM.

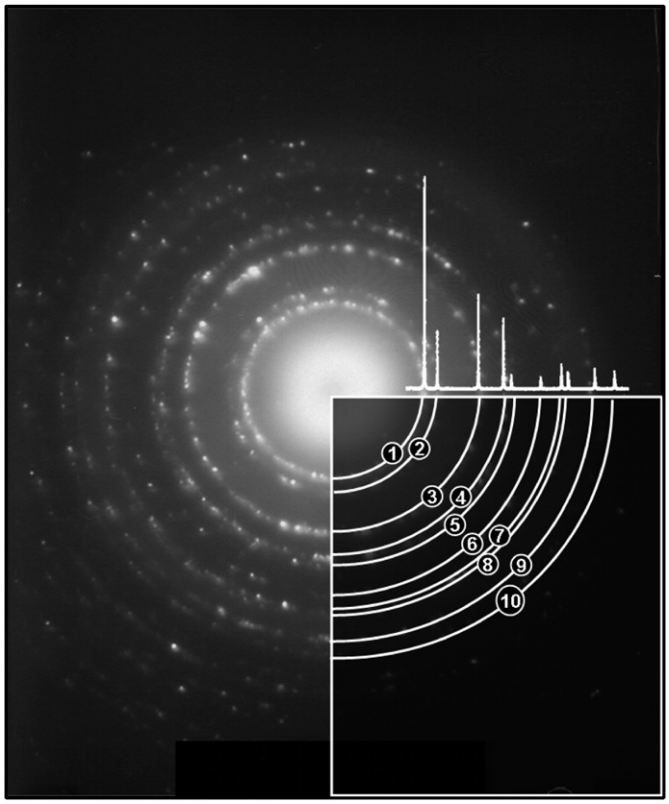

Fig. 4. Electron diffraction pattern of $Ce_{0.9}Gd_{0.1}O_{2-d}$. The planes are (1) (1 1 1), (2) (2 0 0), (3) (2 2 0), (4) (3 1 1), (5) (2 2 2), (6) (4 0 0), (7) (3 3 1), (8) (4 2 0), (9) (4 2 2), (10) (3 3 3). The XRD pattern approximation is also shown.

diffraction pattern obtained by TEM shows the characteristic ring reflexions of a nanometric polycrystalline material while the distances between the planes correspond in a very close approximation with the distances obtained by XRD. Table 1 lists the values of the interplanar distances as estimated with XRD and TEM. The estimated cell parameters are 5.419 Å (XRD) and 5.45 Å (TEM).

Table 1
Interplanar distances as obtained from XRD and TEM

Peak	*d* by XRD (Å)	*d* by TEM (Å)	hkl
1	3.139	3.176	111
2	2.713	2.741	200
3	1.920	1.937	220
4	1.606	1.626	311
5	1.566	1.568	222
6	1.357	1.345	400
7	1.245	1.233	331
8	1.213	1.209	420
9	1.108	1.109	422
10	1.044	1.088	333

The estimated cell parameters are 5.419 and 5.45 Å, respectively.

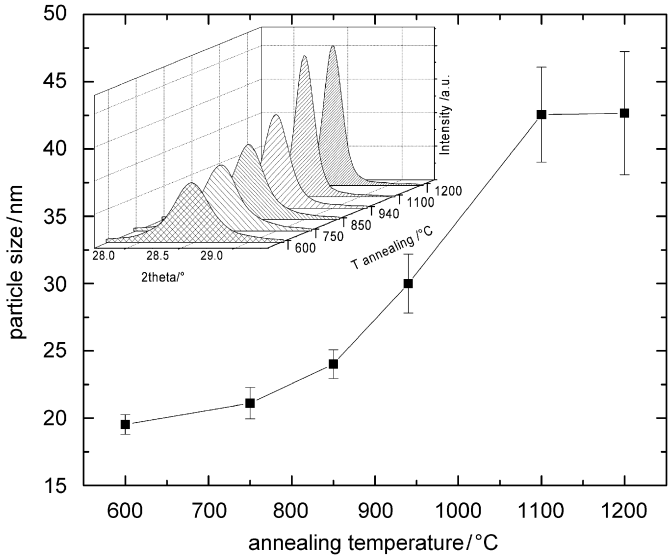

Fig. 5. Particle size as a function of annealing temperature of nanopowders (not pressed). Time of anneal: 3 h. The inset shows the change in width with temperature of the 1 1 1 reflection peak.

As expected, these nanoparticles grow when treated at high temperatures and the effect can be seen in Fig. 5. This figure also shows that there is no further growth above 1100 °C and it seems that a stable size has been reached. It has been shown that grain growth in thin films of Gd-doped CeO_2 stops after 5 h (below 1000 °C) and the grain size remains very stable [31].

4.2. Nanoceramics

The nanopowders obtained have a very good sinterability. A variety of annealing conditions were tested and we found that the best options are a temperature of 1250 °C and dwell times of 5–60 min in air (ca. $p_{O_2} = 0.16$ atm). The densities obtained were above 90% in all cases. Fig. 6 shows a SEM micrograph of a cross section of a dense sample of $Ce_{0.9}Gd_{0.1}O_{2-\delta}$ and we can establish that the grains are all below 250 nm. As seen in the micrograph, no open porosity and/or cracks are visible, a feature that is an important requirement for the application of this ceramic

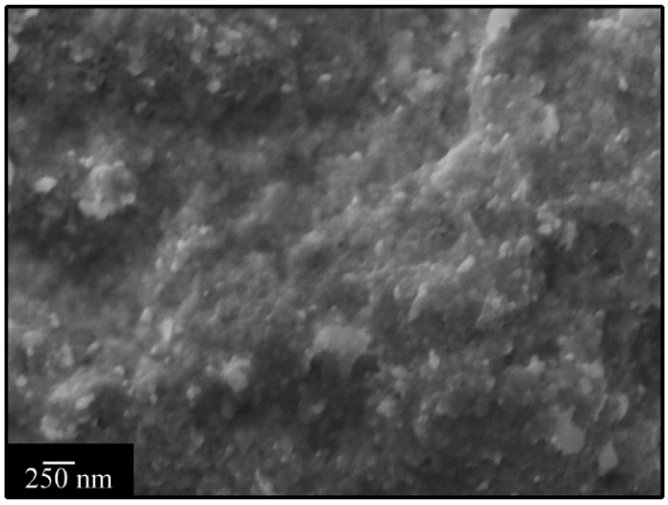

Fig. 6. Cross section of $Ce_{0.9}Gd_{0.1}O_{2-d}$ sample scanned by SEM.

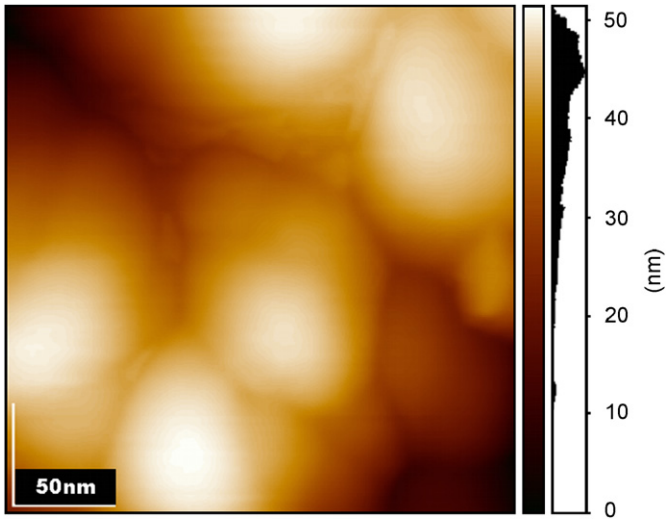

Fig. 7. AFM image of the surface of a sample of $Ce_{0.9}Gd_{0.1}O_{2-d}$ with a 94% of the theoretical density. Grains under 100 nm can be observed.

as a SOFC, SOEC or a separation membrane. In agreement with earlier reports [23,26,27], the densification of doped CeO_2 ceramics to more than 90% can be achieved by sintering powders prepared by combustion synthesis. Fig. 7 displays a better indication of the nanometric size of the grains in the nanoceramic. This picture reveals that some grains are smaller than 100 nm. These grains may not dominate the whole microstructure yet they are probably responsible for the electrical behaviour displayed as will be seen in the next section.

4.3. Electrical conductivity

4.3.1. Impedance spectroscopy

Fig. 8 shows two impedance plots taken at two different atmospheres for two temperatures. The logarithm of the frequency is indicated in these plots as they help us associate a process with the signals. As opposed to previous work in nanoceramics using silver electrodes [20], we observed at least two semicircles using Pt electrodes. In both cases, we can assume that above 1 MHz ($\log f = 6$) the response is due to the bulk as seen at 325 °C in Fig. 8b. We can also assign the signal between ca. 1 and 100 KHz to the grain boundary response. One of the most important features displayed here is a clearly smaller grain boundary response for measurements in argon. On the other hand, the bulk response seems to be the same for both atmospheres at 325 °C but no comparison of the bulk conductivity can be made at higher temperatures as the semicircles are more and more depressed. At low temperatures the grain boundary signal cannot be properly identified as it lies above the equipment measuring capabilities. As the bulk and grain boundaries signals were not always clearly defined in the whole range studied, and as it is not clear yet if an RC-RC is the best equivalent circuit to be applied, we did not separate the two signals with this model. Instead, we used the virtual intercept (ca. 1 KHz in Fig. 8a and 8b) with the real axis and assigned it to the dc conductivity as is customary. This allowed us to compare with the 4-point dc conductivity at higher temperatures in Section 4.3.4.

4.3.2. Polarisation curves

Fig. 9 presents two polarisation curves at high temperature in nitrogen as obtained from the 4-point dc technique. Fig. 9a shows that at 922 °C no polarisation is present and only a very slight change in conductivity as a function of time is observed. However, as the temperature decreases the polarisation increases. Fig. 9b shows considerable polarisation at 809 °C. This phenomenon increases at lower temperatures and therefore no more measurements were performed below 700 °C. Current densities larger than 42 mA cm^{-2} produced a saturation of the current source.

Figs. 10a and 10b show the polarisation curves at 953 and 777 °C in air. Three general comments can be made: firstly, there is no polarisation; secondly, the conductivity does not change as a function of time at these conditions of temperature and atmosphere and finally, a current density higher than 42 mA cm^{-2} can pass through the sample.

From Figs. 9 and 10, we observe clearly that the electrical properties are then definitely affected by the atmosphere. For micrometric-grain sized doped ceria, this effect would not be expected as the bulk conductivity dominates the total conductivity, which is mostly ionic below 1000 °C.

4.3.3. Dc conductivity

Fig. 11 presents the Arrhenius plot for the dc conductivities measured in air and nitrogen atmospheres. A wider temperature range in air could be plotted since the system did not indicate polarisation, as seen in the previous section. On the other hand, the measurements in nitrogen were more restricted in temperature as the samples did not reach stable voltage values below 700 °C. Fig. 11 also contains the conductivities obtained from ac impedance in air and argon atmospheres.

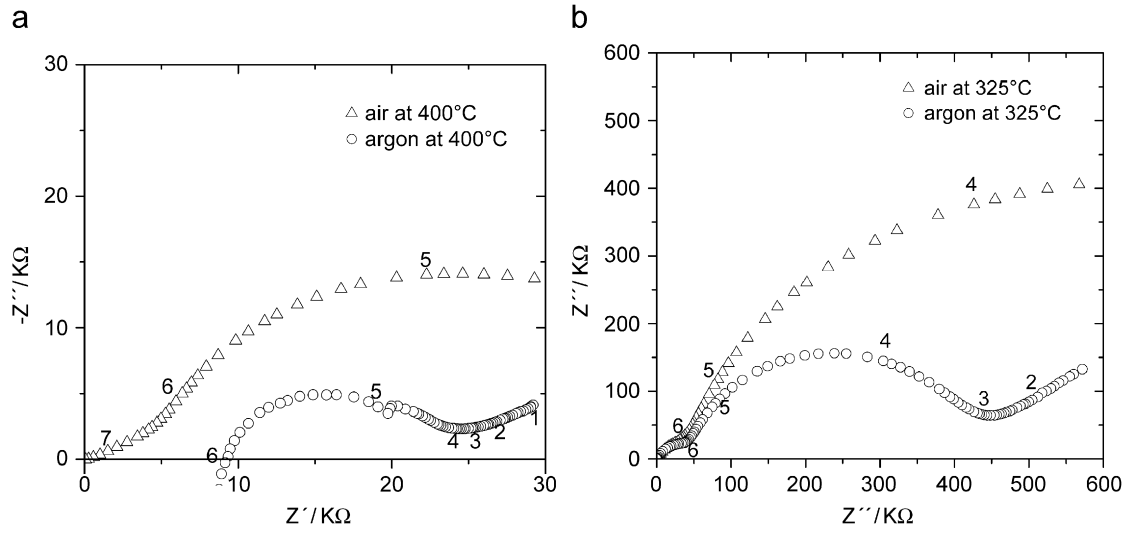

Fig. 8. Impedance plots of $Ce_{0.9}Gd_{0.1}O_{2-d}$ in air (8a) and in argon (8b). The numbers adjacent to the data points indicate the logarithm of the frequency.

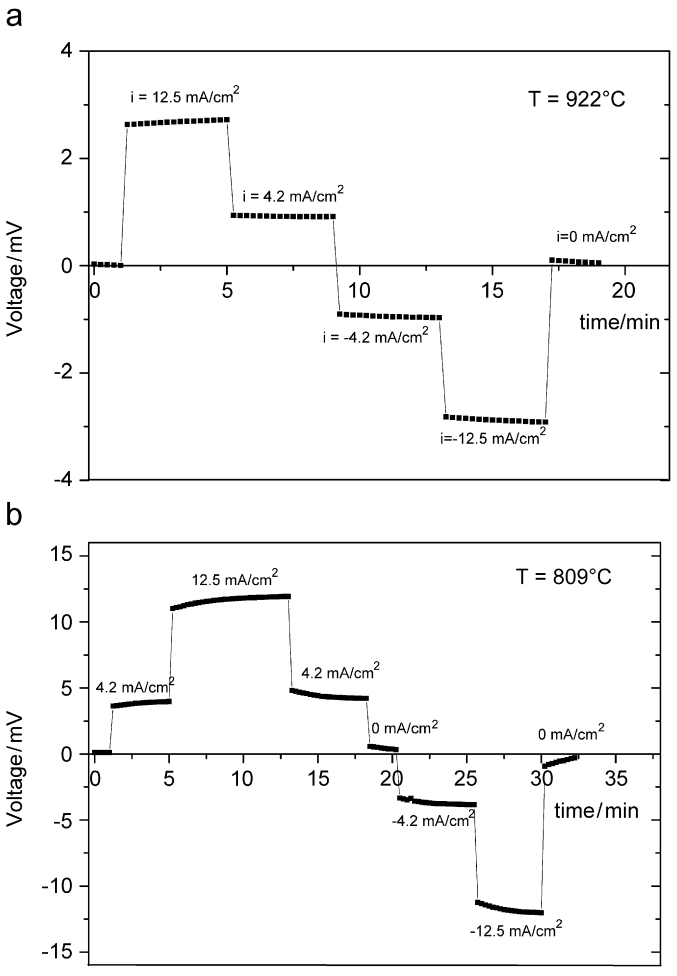

Fig. 9. Polarisation curves at 922 and 809 °C in nitrogen atmosphere.

At high temperature in air the total conductivity displays activation energy of 0.93 eV, a value that is considerably higher than the more accepted value of 0.64 eV for pure bulk material [15]. This latter value is however, related only

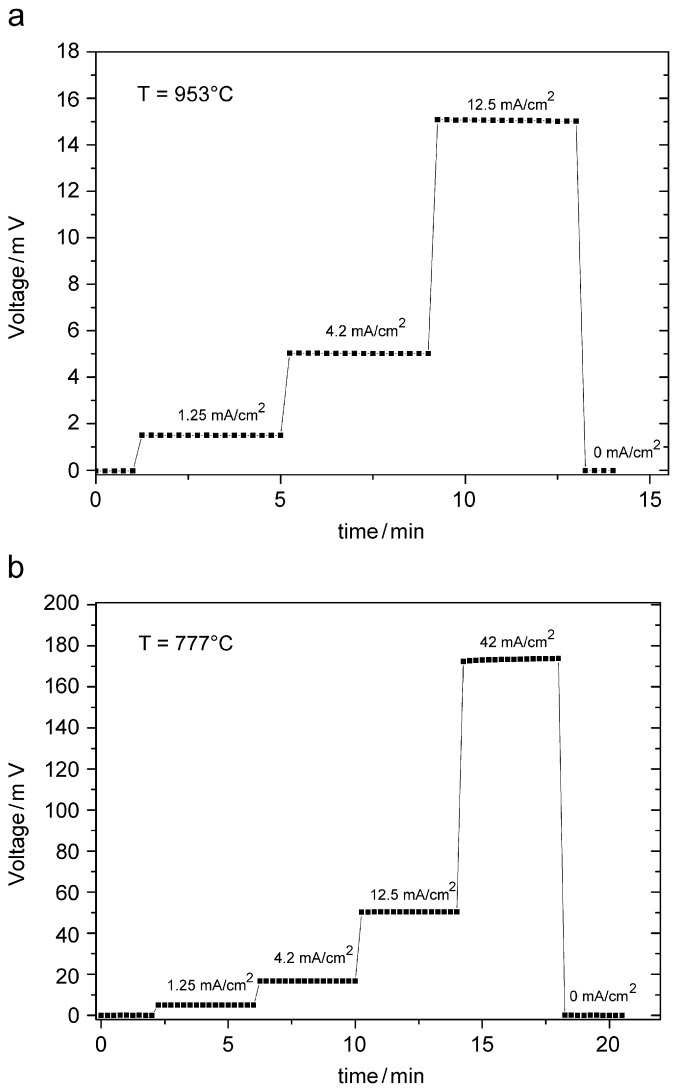

Fig. 10. Polarisation graphs of $Ce_{0.9}Gd_{0.1}O_{2-d}$ in air at 953 and 777 °C.

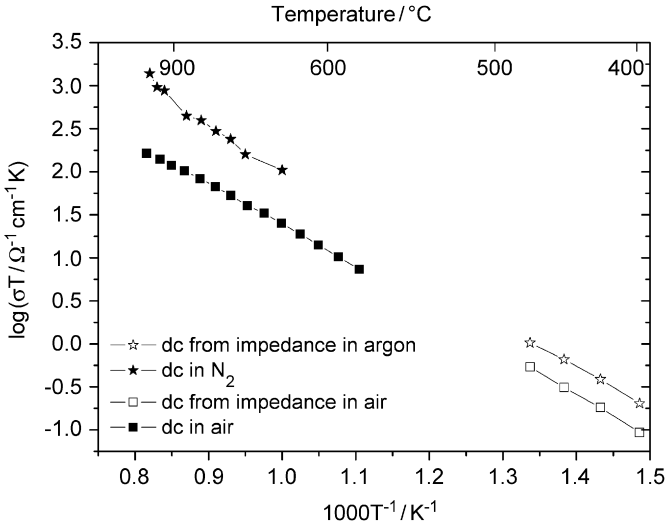

Fig. 11. Arrhenius plot of the dc conductivity of $Ce_{0.9}Gd_{0.1}O_{2-d}$.

to the bulk in a microsized material. Therefore, the values cannot be directly compared but the difference may be a manifestation of an effect of the grain size. It is also observed that the high temperature (dc measurements) and low temperature (impedance measurements) conductivities follow the same trends.

5. Discussion

We have achieved a high density, small grain sized ceramic via the combustion synthesis method. The SEM micrographs (Fig. 6) indicate that the grains are all below 250 nm in size, although a higher resolution was not possible with this technique. The AFM images, however, show that some of the grains are below 100 nm. Studies on the grain growth of Gd-doped CeO_2 seem to indicate that the average size do not increase after 4 h in the temperature range we used [31]. We believe that the electrical measurements are not largely affected by grain growth, and will concentrate on the enhanced conductivity presented by the system under an atmosphere with a relatively low partial pressure of oxygen.

In order to characterise an electrical conductor we need to know the nature of the charge carrier and its mobility. It is important then to determine the nature of the charge carriers. The 4-point dc technique cannot discriminate what type of carrier is responsible for the conductivity but this does allow us to discuss briefly two possibilities: oxygen ions and electrons.

5.1. Oxygen ions vs. electrons

Oxygen ions are the main charge carriers in oxidising atmospheres in micro-grain sized doped ceria materials, as a result of the vacancies generated through doping as indicated in Eq. (1). Usually, above 500 °C the measurement of conductivity by ac impedance yields only the bulk response since the grain boundary is short circuited. This approximation might be valid when the grain boundaries do not represent a large part of the material under measurement and can be considered to be in series with the bulk. Nonetheless, a nanoceramic might have conduction paths along the grain boundaries that cannot be ignored. We have measured 0.93 eV for the total conductivity in air and it is highly likely that, besides the bulk, a grain boundary component is still present. In this respect, it has been suggested that oxygen migration can take place along grain boundaries resulting in an enhanced ionic conductivity in nanoceramics of Y-doped ceria at temperatures below 200 °C in air [20]. A precise determination of the contribution of the oxygen ions to the total conductivity is in progress using the isotopic exchange depth profiling by secondary ion mass spectrometry as performed for the single crystalline material [3].

Reduction can take place in atmospheres with a low partial pressure of oxygen (see Eq. (2)) bringing about mixed ionic-electronic conductivity in micro-sized Gd-doped ceria. In our experiments, we observe an enhancement of conductivity above 700 °C in nitrogen where the system seems to be reducing since the conductivity increases largely and surpasses that of the total conductivity in air. For example, at 930 °C, the conductivity is $0.83\,\Omega^{-1}\,cm^{-1}$ in N_2 ($p_{O_2} = 3.5 \times 10^{-6}$ atm) and $0.38\,\Omega^{-1}\,cm^{-1}$ in air, while the bulk ionic conductivity is estimated as $0.19\,\Omega^{-1}\,cm^{-1}$ [15]. This enhanced conductivity has been observed for Y-doped CeO_2 as well [23]. The fact that the conductivity increases in nitrogen seems to indicate some level of reduction even though such a process in a lattice with oxygen vacancies seems to be in contradiction with simple notions of chemical equilibrium, deducted from Eq. (2). However, that the CeO_2 may be more susceptible to reduction upon doping has been known since the early studies on pure and doped ceria [32]. Furthermore, it has also been reported that it is easier to reduce highly doped ceria than low doped and undoped ceria, especially at temperatures lower than 800 °C [15,33] close to our working temperatures. The determination of Ce^{3+} in the samples under the atmospheres used is of paramount importance. We are currently addressing this problem in Y-doped CeO_2 using electron paramagnetic resonance in samples quenched *ex-situ*.

5.2. Grain boundary vs. bulk transport

The Arrhenius plot in Fig. 11 shows a consistent trend between the total conductivity obtained by ac impedance and the 4-point technique. Furthermore, from the ac impedance we can observe that the semicircle usually associated with the grain boundary resistivity (between 1 kHz and 1 MHz) is clearly smaller in argon than in air. If this trend follows at high temperature, we might think that the grain boundaries form channels along which the charge carriers move. This difference in behaviour with the atmosphere is also clearly displayed in Figs. 9 and 10 in terms of the polarisation; while in air there is no polarisation, in nitrogen the systems takes a longer time to respond and reach a certain level of

equilibrium as though some sort of temperature-dependent atom re-arrangement in the grain boundary or the bulk was taking place. It is interesting to note as well, that when the sample is in N_2, it has a lower capacity to transport charge than when the atmosphere is air. It is not clear at this point; if this polarisation behaviour is an indication that transport takes place along grain boundary when it is electronic. In any case, the Arrhenius plot of Fig. 11 contains the evidence that the conductivity can reach almost an order of magnitude higher in N_2 than in air. This also confirms the results obtained for nanoceramics of Y-CeO_2 [3] although a clear explanation of the transport mechanism is still missing. If a measurable improvement of electronic conductivity was achieved with grain sizes around 100 nm one could expect an even better improvement at smaller sizes. If the ionic conductivity remains high and the electronic conductivity has a higher value in the 500–800 °C temperature range, we may be able to consider this material for a pressure-driven oxygen separation membrane.

6. Conclusions

1. We have successfully prepared nanoparticles of Gd-doped CeO_2 using the combustion synthesis technique. The particle size average is close to 20 nm, calculated using Scherrer's formula, TEM or AFM.
2. This nano-powder possesses excellent sinterability at low temperatures (1250 °C) and short times (<1 h). The ceramics obtained are dense and have grain sizes smaller than 250 nm and the grains can be smaller than 100 nm as observed by AFM.
3. These nano-grains, however, seem to affect the electrical conductivity since we observed a high level of conductivity in N_2 atmospheres compared to air and higher than the most commonly accepted values of ionic conductivity in the bulk.
4. It seems that the increased conductivity has an important electronic contribution and that the grain boundaries play an important role as conduction channels for electrons.
5. The relatively mild reducing condition found for a grain size close to 100 nm led to almost an order of magnitude increase in conductivity, therefore, we may anticipate a larger effect with a smaller grain size. This could be used for the design of materials for separation membranes with a very specific ratio of electronic/ionic conductivity.

Acknowledgments

Financial aid was provided by DGAPA-UNAM under projects PAPIIT- IN105305 and PAPIIT IN-114607. We thank Melisa Angeles-Rosas for support in the experimental section.

References

[1] R.N. Blumenthal, B.A. Pinz, J. Appl. Phys. 38 (5) (1967) 2376–2383.
[2] H.L. Tuller, A.S. Nowick, J. Electrochem. Soc. 122 (2) (1975) 255–259.
[3] E. Ruiz-Trejo, J.D. Sirman, Yu.M. Baikov, J.A. Kilner Solid State Ionics 113–115 (1998) 565–569.
[4] K. Huang, M. Feng, J.B. Goodenough, J. Am.Ceram.Soc. 81 (2) (1998) 357–362.
[5] H.L. Tuller, A.S. Nowick, J. Electrochem. Soc. 126 (2) (1979) 209–217.
[6] H. Yahiro, K. Eguchi, H. Arai, Solid State Ionics 21 (1986) 37–47.
[7] Y.-M. Chiang, E.B. Lavik, I. Kosacki, H.L. Tuller, J.Y. Ying, J. Electroceramic 1 (1997) 7–14.
[8] S. Kim, J. Maier, J. Electrochem. Soc. 149 (2002) J73–J83.
[9] J.H. Hwang, T.O. Mason, Z. Phys. Chem. 207 (1998) 21–38.
[10] A. Tschöpe, E. Sommer, R. Birringer, Solid State Ionics 139 (2001) 255–265.
[11] F.A. Kröger, Chemistry of Imperfect Crystals, North-Holland, Amsterdam, 1964, p 194.
[12] T. Kudo, H. Obayashi, J. Electrochem. Soc. 123 (1976) 415–419.
[13] A. Atkinson, T.M.G.M. Ramos, Solid State Ionics 129 (1–4) (2000) 259–269.
[14] B. Zhu, I. Albinsson, C. Andersson, K. Borsand, M. Nilsson, B.-E. Mellander, Electrochem. Commun. 8 (3) (2006) 495–498.
[15] B.C.H. Steele, Solid State Ionics 129 (2000) 95–110.
[16] U. Nigge, H.-d. Wiemhöfer, E.W.J. Römer, H.J.M. Bouwmeester, T.R. Schulte, Solid State Ionics 146 (2002) 163–174.
[17] H.J. Park, G.M. Choi, J. Eur. Ceram. Soc. 24 (6) (2004) 1313–1317.
[18] O.A. Marina, C. Bagger, S. Primdahl, M. Mogensen, Solid State Ionics 123 (1–4) (1999) 199–208.
[19] A. Tschöpe, J. Electroceram. 14 (2005) 5–23.
[20] M.G. Bellino, D.G. Lamas, N.E. Walsöe de Reca, Adv. Funct. Mater. 16 (2006) 107–113.
[21] T. Suzuki, I. Kosacki, H.U. Anderson, Solid State Ionics 151 (2002) 111–121.
[22] D.R. Ou, T. Mori, F. Ye, M. Takahashi, J. Zou, J. Drennan, Acta Mater. 54 (2006) 3737–3746.
[23] E. Ruiz-Trejo, A. Benítez-Rico, S. Gómez-Reynoso, M. Angeles-Rosas, J. Electrochem. Soc. 154 (4) (2007) A258–A262.
[24] J. Rupp, L. Gauckler, Solid State Ionics 177 (26–32) (2006) 2513–2518.
[25] I. Riess, D. Braunshtein, D.S. Tannhauser, J. Am. Ceram. Soc. 64 (1981) 479–485.
[26] S.V. Chavan, A.K. Tyagi, J. Mater. Res. 19 (2) (2004) 474–480.
[27] T. Mokkelbost, I. Kaus, T. Grande, M.A. Einarsrud, Chem. Mater. 16 (25) (2004) 5489–5494.
[28] A.R. West, Solid State Chemistry, Wiley, Chichester, 1987, p. 174.
[29] N. Sakai, K. Yamaji, Y.P. Xiong, J. Electroceram. 13 (1–3) (2004) 677–682.
[30] LEVM/LEVMW software v8.07, Ross Macdonald, Andriy Gorkovenko, 2006.
[31] J.L.M. Rupp, A. Infortuna, L.J. Gauckler, Acta Mater. 54 (7) (2006) 1721–1730.
[32] G. Brauer, U. Holtschmidt, Z. Anorg. Allg. Chemie 265 (1951) 105–116.
[33] D. Schneider, M. Godickemeier, L. Gauckler, J. Electroceram. 12 (1997) 165–172.